NANO LETTERS

pubs.acs.org/NanoLett

Wiring Nanoscale Biosensors with Piezoelectric Nanomechanical Resonators

Akram S. Sadek,[†,‡] Rassul B. Karabalin,[§] Jiangang Du,[†,§] Michael L. Roukes,[§] Christof Koch,[‡] and Sotiris C. Masmanidis*[,†,§]

[†]Broad Fellows Program in Brain Circuitry, [‡]Computation and Neural Systems, Division of Biology, and [§]Kavli Nanoscience Institute, California Institute of Technology, Pasadena, California 91125

ABSTRACT Nanoscale integrated circuits and sensors will require methods for unobtrusive interconnection with the macroscopic world to fully realize their potential. We report on a nanoelectromechanical system that may present a solution to the wiring problem by enabling information from multisite sensors to be multiplexed onto a single output line. The basis for this method is a mechanical Fourier transform mediated by piezoelectrically coupled nanoscale resonators. Our technique allows sensitive, linear, and real-time measurement of electrical potentials from conceivably any voltage-sensitive device. With this method, we demonstrate the direct transduction of neuronal action potentials from an extracellular microelectrode. This approach to wiring nanoscale devices could lead to minimally invasive implantable sensors with thousands of channels for in vivo neuronal recording, medical diagnostics, and electrochemical sensing.

KEYWORDS NEMS, multiplexing, neural probe

A multitude of promising nanoscale electronic devices have been developed for the implementation of gain,[1] digital logic[2] and analog sensing.[3−5] Yet far less attention has been directed on how to interface systems built from these components with the macroscopic world.[6−9] The top-down wiring problem raises several challenges related to the integration of very large systems with a miniscule footprint. This is especially apparent for sensors based on carbon nanotubes,[3] semiconductor nanowires,[4] nanoelectromechanical systems,[5] and other devices, where the number of readout channels scales in direct proportion to the number of components. Sensor arrays based on these devices have the ability to allow real-time, parallel detection of electrical potentials at thousands of different sites in vivo.[4,10] Interfacing with neural systems in a highly integrated and minimally invasive fashion might also become feasible.[11] However, bulky lithographic wires are currently used to connect with individual devices to extract information and provide power, limiting their integration.

In his lectures on computation, Richard Feynman speculated that the wiring problem might be tackled by an optical interconnection system through free space, acted on by frequency-sensitive components within a system architecture.[12] Here we report on a new paradigm for wiring nanoscale sensor arrays to the macroscopic world, employing frequency-sensitive nanoelectromechanical systems (NEMS) coupled to a single optical output line. Potentially, thousands of sensor channels could be multiplexed in parallel, thereby greatly alleviating the wiring constraints that arise with scaling up device complexity.

The structural element of our technique is a nanoscale piezoelectric beam, as shown in Figure 1a. The devices are fabricated from epitaxially grown GaAs, and as depicted in the cross section in Figure 1b, are comprised of a 200 nm thick pin diode with the n- and p-doped layers connected to the voltage source and ground, respectively. Biasing the pin junction results in an electric field that is concentrated across the ∼50 nm thick charge depletion region. The transverse electric field induces a longitudinal piezoelectric strain within the depletion layer, which can be used to resonantly excite the flexural mode of the beam through application of a radio frequency (rf) drive. The high resistance of the depletion layer means these devices exhibit very low power dissipation during actuation, on the order of 1 nW or less (Supporting Information Figure S1).

As has been reported previously, the resonance frequency of piezoelectrically coupled NEMS resonators is sensitive to an applied electrical potential.[13] This phenomenon arises from the clamped−clamped boundary conditions of the suspended beam structure, which leads to the conversion of piezoelectric strain into compressive or tensile stress, and modulation of the natural frequency of the structure. Importantly, this shift is linearly proportional to applied voltage with a slope of approximately 40 kHz per volt for these fabricated devices (Supporting Information Figure S2). Here we use this frequency tuning effect to transduce time-varying electrical potentials that might, for example, originate from nanoscale sensors of electrophysiological activity. Normally, resonance frequency shifts in NEMS are extracted via a phase-locked loop.[5] In contrast, to facilitate real-time readout our scheme indirectly monitors

* To whom correspondence should be addressed. E-mail: sotiris@caltech.edu.
Received for review: 01/22/2010
Published on Web: 04/09/2010

DOI: 10.1021/nl100245z | *Nano Lett.* **2010,** *10,* 1769–1773

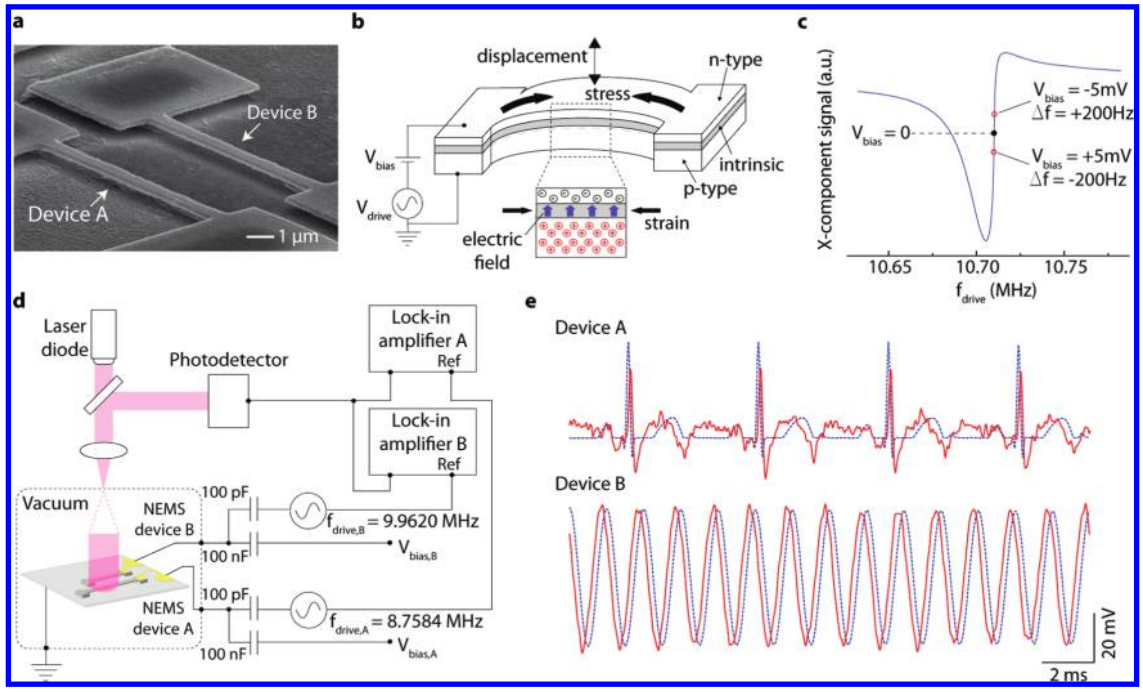

FIGURE 1. Piezoelectric NEMS and nanomechanical Fourier transform. (a) Dual piezoelectric NEMS devices A and B, spaced 4 μm apart. The dimensions of the beams are (length, width, thickness) = (9, 0.8, 0.2) and (8.5, 0.8, 0.2) μm for A and B, respectively. (b) An electric field across the pin junction generates longitudinal piezoelectric strain. An actuating radiofrequency potential, V_{drive}, drives the beam to resonance. A slowly varying potential, V_{bias}, modulates the baseline stress in the beam and tunes the resonance frequency. (c) X-component of the resonance plot for device C when it is driven nonlinearly. A lock-in amplifier locks on to the steepest point (black). When V_{bias} is applied the resonance plot shifts along the frequency axis, and the lock-in point varies in amplitude (red circles). In this manner, signals are encoded as spectral amplitude variations at a specific frequency and can be transduced in real-time. (d) Schematic of experimental setup to demonstrate multiplexing through a nanomechanical transducer. All mechanical displacement is read out via a common optical transmission path. (e) Signals (red) recovered from multiplexed optical readout of devices A and B by means of lock-in amplification. The original corresponding bias signal on each device is represented by a dashed blue line. The small phase offset originates from the low-pass RC filter formed by the signal output impedance and large parasitic capacitance at the device wirebond contact region. Results represent 450 averages.

frequency by operating the resonator at a fixed rf driving frequency, and tracks variations in oscillation amplitude that are manifested as the bias signal shifts the position of the resonance peak. In the small bias regime, the demodulated signal amplitude can be expressed as

$$A(t) = -[d_{31}\eta(Q, V_{drive})/2\pi h^2]\sqrt{3E/\rho}V_{bias}(t) \qquad (1)$$

where $\eta(Q, V_{drive})$ is the slope of the resonance curve represented in Figure 1c, which is dependent on the quality factor and drive amplitude; E, ρ, and d_{31} are the Young's modulus, density, and transverse piezoelectric coefficient of the structural material, and h is the device thickness.[13,14] As eq 1 suggests, reducing the device thickness to nanoscale dimensions is important for maximizing sensitivity. In addition, we have found that sensitivity can be further enhanced by operating the resonator in the regime of nonlinear bistability (Figure 1c) in which the slope η is increased. It should be emphasized that while nonpiezoelectric NEMS devices can also transduce an applied bias through electrostatic coupling, their tuning action is nonlinear and thus less suitable for recovery of analog signals.[15–17]

The fundamental frequency of a NEMS resonator can be tailored through its length. An array of resonators of differing lengths can then be used to produce a nanomechanical Fourier transform, encoding signals in the time domain into spectral amplitude variations using the modulation scheme described. Optical readout techniques can subsequently monitor the oscillation amplitude of the resonators concurrently through a single transmission channel, provided the devices are spaced close together. Downstream demodulation of the optical signal can recover and uniquely identify the origin of a signal based on the rf actuation frequency. NEMS resonators can be operated at frequencies ranging from several megahertz to over one gigahertz,[18] suggesting thousands of different channels could be encoded onto a single output (see Supporting Information).

We demonstrate the multiplexing technique using laser interferometry[19] to monitor variations in transverse oscillation amplitude from the two closely spaced NEMS devices (A and B) depicted in Figure 1a. They have lengths of 9.0 and 8.5 μm, and resonate at 8.758 and 9.962 MHz, respectively. The experimental setup is illustrated in Figure 1d (see Supporting Information for detailed methods). The laser was focused to a diameter of ~10 μm, allowing concomitant

DOI: 10.1021/nl100245z | *Nano Lett.* **2010,** *10,* 1769–1773

observation of both resonant structures. The devices were operated in vacuo to maintain high quality factor and resonance frequency stability. Each device was capacitively coupled to two signals, (i) the rf driving potential V_{drive}, whose frequency corresponded to the region of highest X-quadrature slope in Figure 1c, and (ii) the bias signal used to simulate the output of an analog electrical sensor. The single-channel photodetector signal was demodulated using lock-in amplifiers referred to f_{drive} of each device. Figure 1e shows the demodulated signals transduced from devices A and B. We were able to closely reproduce the fine structure of the pulse applied to device A and the sinusoidally varying signal on device B. We verified that the cross-talk between signals applied on each device did not exceed ~2% at 1 kHz (Supporting Information Figure S3), despite the close spacing of the beams. It was possible to accurately track bias signals for tens of minutes without adjusting the rf driving potential parameters. Over longer time scales we observed drift that was compensated by a single-shot manual recalibration of f_{drive}.

Figure 2a plots the dependence of the transduced signal amplitude of device A on the rf drive voltage under a constant bias at 1 kHz. The inset shows resonance curves at representative values of V_{drive}. It is evident that the system's response improves as a result of actuating the resonator in the regime of nonlinear bistability. Above a critical point corresponding to strong nonlinear drive the readout appears to become unstable, as suggested by the abrupt decrease in response. The optimal response for this particular device occurs just below the instability regime at $V_{drive} \approx 50\ mV_{rms}$. We verified that the noise did not appreciably change below the instability (Supporting Information Figure S4) and thus confirmed that the optimal signal-to-noise ratio (SNR) is achieved by actuating the NEMS devices at levels slightly lower than the critical point. We next varied the bias amplitude under fixed V_{drive} and observed a linear response at low bias levels (Figure 2b). Note that the earlier onset of nonlinear response in device A compared to that of device B is due to its higher quality factor.

A characteristic of the nonlinear driving regime of the nanomechanical system is a greater attenuation of signal response at high bias frequency. Figure 2c characterizes the frequency response for devices A and B under varying drive amplitude. For both devices the response curve remains flat at low V_{drive}, but becomes progressively biased toward lower frequencies as V_{drive} approaches the critical point. The attenuation effect is more marked for the device with higher quality factor. These observations appear to be a manifestation of the ring-down time of the resonator ($\sim Q/4\pi f_0$).[20] Our results closely agree with the theoretical prediction that the greatest voltage sensitivity of this system is achieved just below the critical point, but that this operating regime exhibits the longest ring-down time and hence smallest bandwidth.[21] For electrical sensors requiring both high sensitivity and bandwidth, nanomechanical transduction would therefore necessarily rely on the use of higher operating frequency NEMS resonators. As the piezoelectric device scheme is linear, the original bias signals can be recovered through deconvolution with the frequency response characteristic of each device. The particular application of the system will determine the device quality factor specification

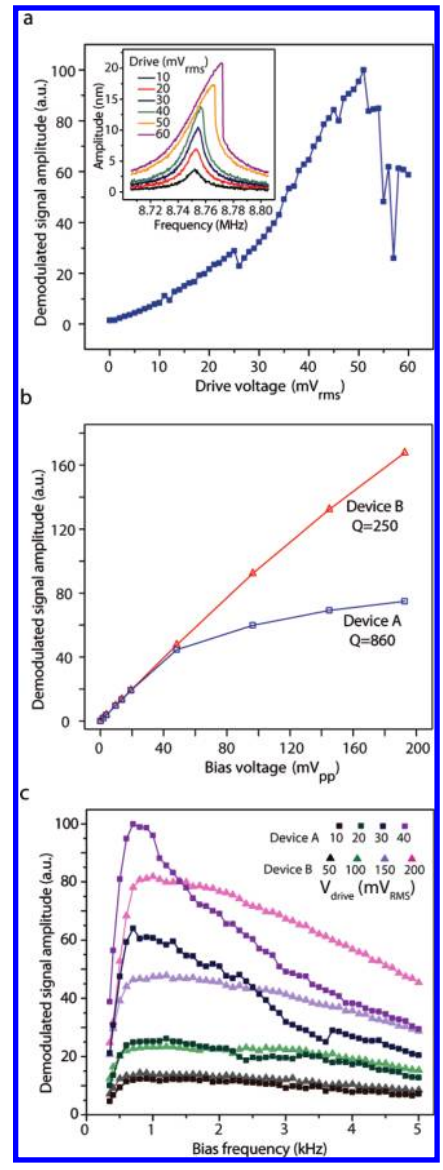

FIGURE 2. Device characterization. (a) Enhancement of device A's transduced signal with increasing rf drive amplitude. The bias signal amplitude and frequency were set to 30 mV_{pp} and 1 kHz respectively. The inset shows resonance plots of the flexural oscillation amplitude at representative drive levels. (b) Nanomechanically transduced signal amplitude of a 1 kHz sinusoidal signal applied to devices A and B as a function of the applied bias amplitude. The actuation parameters were $V_{drive,A} = 40\ mV_{rms}$ and $V_{drive,B} = 200\ mV_{rms}$. (c) Bias frequency response of devices A and B at various driving amplitudes in the linear and nonlinear NEMS actuation regime. Note that the notch at $f_{bias} < 500$ Hz is due to our applied high-pass filter and is not an intrinsic nanomechanical effect. V_{bias} was set to 30 mV_{rms} for both devices. For all plots the demodulated signal amplitude was averaged 2500 times.

DOI: 10.1021/nl100245z | *Nano Lett.* **2010,** *10,* 1769–1773

and driving regime. This is due to the trade-off in ultimate wiring density, signal bandwidth, sensitivity, and SNR that arises from these factors. Greater quality factor increases the SNR and the number of channels that can be multiplexed in a given frequency band, but may limit the bandwidth and dynamic range of the transduced bias signal. Furthermore, stronger nonlinear drive increases SNR but impacts the bandwidth.

Some applications of sensors require measurement of low amplitude, low SNR bias signals. This challenge is particularly salient in the monitoring of electrophysiological activity in the brain using multisite extracellular electrode arrays. Such recordings are an invaluable method for studying functional properties of the intact brain from the microcircuit to systems level.[22] Recordings can be carried out with an implantable neural probe that connects a grid of microscale electrodes to amplifying electronics via wires spanning the length of the probe. As the complexity of such neural interfaces increases, the primary size-determining factor of the devices becomes the interconnecting wires, and an arbitrary reduction of wire width is not necessarily a practical solution.[23]

Application of our technique has the potential to enable fabrication of much higher density and less invasive neural interfaces. We therefore report on the effectiveness of transducing extracellular action potentials via a NEMS-neural probe interface. A stand-alone resonator (device C) was coupled to a recording site on the probe shown in Figure 3a.[24] The implantable section of the probe was inserted into a locust thoracic ganglion induced to sustain rhythmically discharging neurons (see Supporting Information for a detailed description of the methodology).[25,26] The electrode was connected to the resonator via a blocking capacitor, which prevented dc photoelectric charge generated at the GaAs device from coupling to the electrode. A parallel connection went to an extracellular amplifier for cross-validation of the nanomechanically transduced signal. Extracellular neuronal action potentials were identified from the amplifier recording, allowing spike-triggered averages to be obtained on the synchronously collected measurements from the NEMS and electronic amplifier. The mean waveform of an 80 μV_{pp} spike is depicted in Figure 3b and is simultaneously observed at the demodulated output of the NEMS resonator. We confirmed the mechanical origin of the demodulated signal by verifying that the action potential is no longer measured if the resonator is detuned by 1 % from its fundamental frequency.

The SNR is small when transducing signals as diminutive as those from extracellular microelectrodes. To achieve a measurable action potential waveform it was necessary to average the NEMS signal from 5000 spike events. The best noise performance we could achieve was 400 μV_{rms} referred to the microelectrode input (in the frequency band of 350 to 3000 Hz), as shown by measurements displayed in Figure 3c. Moreover, we verified that over 80 % of the measured

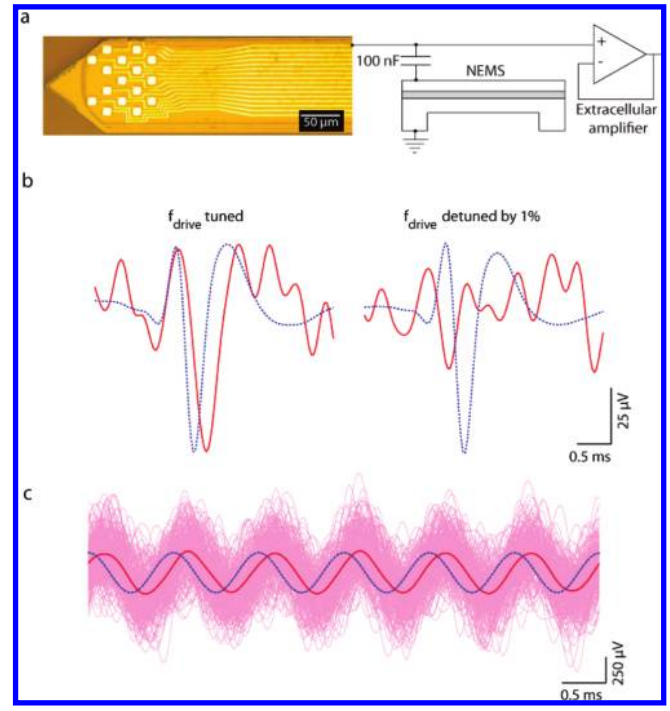

FIGURE 3. Nanomechanical transduction of extracellular action potentials. (a) Neural probe used in our experiments. A single channel was connected in parallel to NEMS device C (length, width, thickness) = (8, 0.8, 0.2) μm and an extracellular amplifier. (b) Detection of extracellular action potentials in a locust ganglion preparation using the setup in panel a. Demodulated signals from the NEMS device are shown in red, and the corresponding signal recorded by the amplifier is indicated by dashed blue lines. Mechanical readout was confirmed through the extinction of spike detection upon detuning the resonator by 100 kHz (i.e., ~1%). Data is averaged over 5000 spike-triggered events. (c) The neural probe coupled to the NEMS device was used to detect an artificially generated signal in saline solution. Nanomechanical signal appears in red (250 averages). Individual, unaveraged NEMS traces are indicated in magenta. The averaged trace from the extracellular amplifier is in dashed blue. The SNR of the transduced signal is ~1:1.

noise was not intrinsic to the devices but appeared to originate in the external demodulation electronics (Supporting Information Figures S5, S6). Fundamentally, the ability to discriminate voltage shifts by a piezoelectric NEMS resonator will be limited by thermomechanical fluctuations. For device C, we estimate a thermomechanical frequency noise of ~2.4 Hz in the 350 to 3000 Hz band, which corresponds to an effective measurement limit of 60 μV_{rms} (Supporting Information eqs S2−S4).[20,27] Conventional electronic amplifiers designed for electrophysiological recording have a noise floor approaching 1 μV_{rms}.[28] To move toward the same performance level, about 2 orders of magnitude in noise reduction and SNR enhancement is required for piezoelectric NEMS. We envision several possible approaches for overcoming these challenges: the use of lighter, stiffer, and stronger piezoelectrically coupled materials, such as aluminium nitride, would both reduce the noise floor and improve SNR; reduction of parasitic capacitance through miniaturization of device contacts would ameliorate signal attenuation effects; improvement in resonator quality factor

DOI: 10.1021/nl100245z | *Nano Lett.* **2010,** *10,* 1769–1773

would boost SNR; and the deployment of arrays of identical NEMS devices would help remove thermomechanical noise limits through signal averaging.

In our present scheme, two physical wires are required in addition to the optical interconnect for communication with the external environment; a ground terminal and a path carrying the multifrequency AC drive generated externally. However recent progress with on-chip waveguide fabrication and evanescent wave optical detection schemes[29,30] raise the intriguing possibility that these techniques could be integrated with piezoelectric NEMS. Moreover, electronic circuits mimicking the function of the human cochlea could provide a compact method of demodulating signals from our system.[31] An interface combining all these novel attributes might make feasible the development of miniature nanoscale integrated sensors that could be positioned at any place in the human body and be used to extract vast amounts of information in real-time and with single-cell fidelity.

Acknowledgment. We thank I. De Vlaminck, W. van de Graaf, S. Degroote, and G. Borghs for the epitaxial GaAs substrates, G. Laurent for assistance with locust preparations and discussions, R. R. Harrison for the extracellular electronic amplifiers, M. R. Freeman for support with optical interferometry, and H. A. Lester for discussions. Device fabrication was carried out at the Kavli Nanoscience Institute, Caltech, and the NNIN Nanofabrication facility, UC Santa Barbara. This work was supported by the Broad Foundation under the Broad Fellowship Program in Brain Circuitry.

Supporting Information Available. Materials and Methods and Supporting Figures. This material is available free of charge via the Internet at http://pubs.acs.org.

REFERENCES AND NOTES

(1) Joachim, C.; Gimzewski, J. K. *Chem. Phys. Lett.* **1997**, *265*, 353–357.
(2) Bachtold, A.; Hadley, P.; Nakanishi, T.; Dekker, C. *Science* **2001**, *294*, 1317–1320.
(3) Kong, J.; Franklin, N. R.; Zhou, C. W.; Chapline, M. G.; Peng, S.; Cho, K. J.; Dai, H. J. *Science* **2000**, *287*, 622–625.
(4) Cui, Y.; Wei, Q.; Park, H.; Lieber, C. M. *Science* **2001**, *293*, 1289–1292.
(5) Ekinci, K. L.; Huang, X. M. H.; Roukes, M. L. *Appl. Phys. Lett.* **2004**, *84*, 4469–4471.
(6) Zhong, Z.; Wang, D.; Cui, Y.; Bockrath, M. W.; Lieber, C. M. *Science* **2003**, *302*, 1377–1379.
(7) Beckman, R.; Johnston-Halperin, E.; Luo, Y.; Green, J. E.; Heath, J. R. *Science* **2005**, *310*, 465–468.
(8) Wang, Z. L.; Song, J. *Science* **2006**, *312*, 242–246.
(9) Walt, D. R. *Nat. Mater.* **2002**, *1*, 17–18.
(10) Zheng, G.; Patolsky, F.; Cui, Y.; Wang, W. U.; Lieber, C. M. *Nat. Biotechnol.* **2005**, *23*, 1294–1301.
(11) Patolsky, F.; Timko, B. P.; Yu, G. H.; Fang, Y.; Greytak, A. B.; Zheng, G. F.; Lieber, C. M. *Science* **2006**, *313*, 1100–1104.
(12) Feynman, R. P. *Feynman Lectures on Computation*; Addison-Wesley: Reading, MA, 1996.
(13) Masmanidis, S. C.; Karabalin, R. B.; De Vlaminck, I.; Borghs, G.; Freeman, M. R.; Roukes, M. L. *Science* **2007**, *317*, 780–783.
(14) Timoshenko, S. *Vibration Problems in Engineering*, 4th ed.; Wiley: New York, 1974.
(15) Cleland, A. N.; Roukes, M. L. *Nature* **1998**, *392*, 160–162.
(16) Truitt, P. A.; Hertzberger, J. B.; Huang, C. C.; Ekinci, K. L.; Schwab, K. C. *Nano Lett.* **2007**, *7*, 120–126.
(17) Unterreithmeier, Q. P.; Weig, E. M.; Kotthaus, J. P. *Nature* **2009**, *458*, 1001–1004.
(18) Huang, X. M. H.; Feng, X. L.; Zorman, C. A.; Mehregany, M.; Roukes, M. L. *New J. Phys.* **2005**, *7*, 247.
(19) Carr, D. W.; Craighead, H. G. *J. Vac. Sci. Technol., B* **1997**, *15*, 2760–2763.
(20) Ekinci, K. L.; Yang, Y. T.; Roukes, M. L. *J. Appl. Phys.* **2004**, *95*, 2682–2689.
(21) Buks, E.; Yurke, B. *Phys. Rev. E* **2006**, *74*, No. 046619.
(22) Buzsáki, G. *Nat. Neurosci.* **2004**, *7*, 446–451.
(23) Najafi, K.; Ji, J.; Wise, K. D. *IEEE Trans. Biomed. Eng.* **1990**, *37*, 1–11.
(24) Du, J.; Riedel-Kruse, I. H.; Nawroth, J. C.; Roukes, M. L.; Laurent, G.; Masmanidis, S. C. *J. Neurophysiol.* **2009**, *101*, 1671–1678.
(25) Ryckebusch, S.; Laurent, G. *J. Neurophysiol.* **1994**, *72*, 2771–2785.
(26) Rutishauser, U.; Schuman, E. M.; Mamelak, A. N. *J. Neurosci. Methods* **2006**, *154*, 204–224.
(27) Tilmans, H. A. C.; Elwenspoek, M.; Fluitman, J. H. J. *Sens. Actuators, A* **1992**, *30*, 35–53.
(28) Harrison, R. R.; Charles, C. A.; IEEE, J. *Solid-State Circuits* **2003**, *38*, 958–965.
(29) Li, M.; Pernice, W. H. P.; Xiong, C.; Baehr-Jones, T.; Hochberg, M.; Tang, H. X. *Nature* **2008**, *456*, 480–484.
(30) De Vlaminck, I.; Roels, J.; Taillaert, D.; Van Thourhout, D.; Baets, R.; Lagae, L.; Borghs, G. *Appl. Phys. Lett.* **2007**, *90*, 233116.
(31) Mandal, S.; Zhak, S. M.; Sarpeshkar, R. *IEEE J. Solid-State Circuits* **2009**, *44*, 1814–1828.

DOI: 10.1021/nl100245z | *Nano Lett.* **2010,** *10,* 1769–1773